# *Locally coordinated synaptic plasticity of visual cortex neurons in vivo*

HHS Public Access

Author manuscript

*Science*. Author manuscript; available in PMC 2019 February 07.

Published in final edited form as:

*Science*. 2018 June 22; 360(6395): 1349–1354. doi:10.1126/science.aao0862.

# Locally Coordinated Synaptic Plasticity of Visual Cortex Neurons *in vivo*

**Sami El-Boustani**[#1,2,*], **Jacque P K Ip**[#1], **Vincent Breton-Provencher**[1], **Graham W Knott**[3], **Hiroyuki Okuno**[4,5], **Haruhiko Bito**[6], and **Mriganka Sur**[1,*]

[1]Department of Brain and Cognitive Sciences, Picower Institute for Learning and Memory, Massachusetts Institute of Technology, Cambridge, Massachusetts 02139, USA [2]Current affiliation: Brain Mind Institute, School of Life Sciences, Ecole Polytechnique Fédérale de Lausanne, Lausanne 1015, Switzerland [3]Bio Electron Microscopy Laboratory, School of Life Sciences, École Polytechnique Fédérale de Lausanne, Lausanne 1015, Switzerland [4]Medical Innovation Center, Kyoto University Graduate School of Medicine, Sakyo-ku, Kyoto 606-8507, Japan [5]Department of Biochemistry and Molecular Biology, Kagoshima University, Graduate School of Medical and Dental Sciences, 8-35-1 Sakuragaoka, Kagoshima 890-8544, Japan [6]Department of Neurochemistry, Graduate School of Medicine, The University of Tokyo, Hongo 7-3-1, Bunkyo-ku, Tokyo 113-0033, Japan

[#] These authors contributed equally to this work.

## Abstract

Plasticity of cortical responses *in vivo* involves activity-dependent changes at synapses, but the manner in which different forms of synaptic plasticity act together to create functional changes in neurons remains unknown. We found that spike timing-induced receptive field plasticity of visual cortex neurons is anchored by increases in synaptic strength of identified spines. This is accompanied by a decrease in the strength of adjacent spines on a slower time scale. The locally coordinated potentiation and depression of spines involves prominent AMPA receptor redistribution via targeted expression of the immediate early gene Arc. Hebbian strengthening of activated synapses and heterosynaptic weakening of adjacent synapses thus co-operatively orchestrate cell-wide plasticity of functional neuronal responses.

## One Sentence Summary:

[*]Corresponding author: Mriganka Sur (msur@mit.edu) and Sami El-Boustani (elbousta@mit.edu).

Author Contribution:

S.E.B., J.P.K.I. and M.S conceived experiments. S.E.B. performed single-cell electroporation. S.E.B. and J.P.K.I. performed surgeries and carried out *in vivo* experiments. S.E.B performed data analysis. M.S. and J.P.K.I. contributed to analysis of experiments. V.B-P. performed intracellular recordings *in vivo* and eye tracking controls. G.W.K. performed the electron microscopy and analysis. H.O. and H.B. designed and provided the Arc-EGFP plasmid and 260 the CaMKIIβ shRNA and controls. S.E.B., J.P.K.I., V.B-P. and M.S. wrote the paper.

**Competing interest:** Authors declare no competing interests.

Data Availability:

All data needed to evaluate the conclusions in the paper are present in the paper or the Supplementary Materials, or are available at www.surlab.org. pGL4.11-Arc7000-mGFP-Arc-UTRs, CaMKIIβ shRNA vector and control shRNA vector are available from Prof. Haruhiko Bito under a material agreement with the University of Tokyo.

Local strengthening and weakening of synapses, mediated by Arc, reorganizes responses on dendrites to mediate functional plasticity of neuronal responses *in vivo*.

Neuronal circuits in the brain are subject to changes driven by sensory inputs (1, 2) or motor learning (3–5), causing cells to modify their responses to individual inputs while maintaining a stable level of activity (6). Homeostatic plasticity stabilizes the output firing rate of single neurons by uniformly scaling up or down the strength of all synapses (6, 7). Other forms of compensatory plasticity can also act locally at dendritic stretches (8–14) or even at single synapses (15–17). Synaptic potentiation at specific dendritic locations could be coordinated with heterosynaptic depression of nearby synapses within short stretches of the same dendrite to co-operatively implement functional plasticity of single cell responses (18). It is unknown whether locally coordinated synaptic plasticity occurs *in vivo*, and whether it has a role in shaping neuronal responses.

Cortical plasticity induced by sensory deprivation or enrichment (2) results in largescale functional and structural changes across many neurons and synapses. We developed a controlled paradigm for inducing plasticity at identified synapses on single neurons in the primary visual cortex (V1) of awake juvenile mice (P28-P35). We reasoned that pre-before-post pairing at specific synapses, via visual stimuli presented at a target location closely followed by channelrhodopsin-2 (ChR2) driven spiking of an individual neuron, would induce Hebbian potentiation of excitatory synapses responding to the target stimulus and consequently shift the receptive field at the soma (Fig. 1A-B). We characterized excitatory synaptic inputs to V1 layer 2/3 neurons in response to sparse noise stimuli (19) (Fig. 1C-E). Evoked EPSCs typically responded to stimulus onset or offset (Fig. 1F). Onset responses lasted for about 200 ms with a peak response at 65–130 ms (mean 96.3±7.4 ms, n=8 neurons). To ensure that the peak synaptic input leads the ChR2 action potential, we induced postsynaptic spiking 150 ms after visual stimulus onset to potentiate responses to the target stimulus and avoid post-before-pre pairing. Such ChR2-induced spiking corresponded to a peak EPSP–spike timing difference of 20–85 ms, which overlaps with time windows used in previous studies to induce response potentiation (20, 21).

To induce and measure receptive field plasticity over extended periods of time, we electroporated the calcium indicator mRuby2-P2A-GCaMP6s (22) and ChR2-mCherry (23) in single-neurons (19) (Fig. 1G,H). ChR2 allowed precise control of neuronal spikes (Fig. 1I, n=7 neurons, number of spikes/pulse = 1.2±0.32). We used the GCaMP6s signal to map receptive fields measured at the soma (Fig. 1J-K, Fig. S1A-B). We then determined a target location close to the peak receptive field response location. Repeated presentations of the target stimulus were paired with single blue light pulses to elicit ChR2 spikes (60 pairings). Receptive fields were measured again 1-to-2 hours post-pairing. For most neurons, the receptive field center-of-mass shifted toward the target stimulus (Fig. 1K-L). These changes were not observed when ChR2 stimulation was not paired with the target stimulus (19) (Fig. 1L). Receptive field shifts could not be explained by changes in eye position (Fig. S2) and did not induce functional changes in the network (Fig. S3). Receptive field shifts could also be achieved with other pairing rates and durations (Fig. S4).

We next investigated the structural basis of receptive field plasticity at the synaptic level. We used dendritic spine volume changes as a structural proxy for long-term potentiation or depression (24–26). By comparing dendritic spines pre- and post-pairing, we observed bi-directional volume changes within dendritic stretches (Fig. 2A). These changes were not caused by drifts in the imaging planes (Fig. S5). Spines exhibiting structural long-term potentiation (sLTP) or depression (sLTD) were compared to control experiments in the absence of ChR2 (ChR2-; Fig. 2B-C). We quantified changes in spine volume using the normalized difference (δV) between the integrated spine fluorescence signal relative to shaft pre- and post- pairing, and defined a threshold for pairing-induced sLTP and sLTD in ChR2+ neurons ($\delta V = \pm 0.25$, corresponding to spines that exceeded the $97^{th}$ percentile of the ChR2- distribution; Fig. S6). We then backtracked the temporal evolution of significantly potentiated or depressed spines (Fig. 2D). sLTP spines rapidly increased in volume right after pairing followed by a moderate increase over the next two hours. In contrast, sLTD spines showed an initial small decrease in volume that was amplified over the following two hours until the average volume change for sLTD and sLTP spines became approximately balanced. The density of sLTD spines was significantly correlated with, and was greater than, the density of sLTP spines in individual dendrites (Fig. 2E). sLTD spine density was significantly larger at short sLTP-sLTD distances (19) indicating that sLTD spines were preferentially clustered around sLTP spines (Fig. 2F).

We also reconstructed stretches of dendrite from ChR2+ and ChR2− neurons with electron microscopy (EM) (Fig. 2G, J), and compared spines that were well-isolated in two-photon images (19). All two-photon imaged spines on these dendrites were identified by EM. For both the ChR2+ and ChR2− dendrite, EM spine volumes were highly correlated with the spine fluorescence signal post-pairing (Fig. 2H, K). Consistent with the observation that structural plasticity caused by pairing resulted in both increase and decrease of spine volumes in ChR2+ neurons whereas volumes remained stable in ChR2− neurons, pre-pairing signals showed significantly larger dispersion around the best fit for the ChR2+ dendrite (Fig. 2H) but were equivalent to post-pairing signals for the ChR2− dendrite (Fig. 2K). EM spine volume was highly correlated with synaptic surface area, consistent with the hypothesis that synaptic weight is reflected in spine volume changes (Fig. 2I, L and Fig. S7).

We investigated the functional signature associated with structural changes to evaluate if they were consistent with receptive field plasticity measured at the soma. GCaMP6s activity in individual spines was used to measure input-specific receptive fields (Fig. 3A-C). Spine receptive fields were heterogeneously distributed along dendritic stretches (Fig. S8). We hypothesized that sLTP spines should have their receptive field centers overlapping the visual target because of Hebbian plasticity, whereas nearby sLTD spines would have receptive field centers located away from the target because of heterosynaptic, potentially co-operative, plasticity. Spines with receptive fields overlapping the target stimulus indeed increased in volume (Fig. 3D,E), whereas neighboring spines with receptive fields away from the target were reduced (Fig. 3D,F). Structural changes were accompanied by consistent changes in GCaMP6s signal amplitude (Fig. S9). The average receptive field for sLTP spines was sharp and centered on the target whereas the average receptive field for sLTD spines was distributed broadly away from and around the target (Fig. 3G). The distribution of sLTP and sLTD spines as a function of their receptive field distance from the

target confirmed that as distance increased, the effect on spine size shifted from sLTP to sLTD (Fig. 3H).

We next electroporated an AMPA receptor (AMPAR) subunit 1 tagged with a pH-sensitive form of GFP (Super Ecliptic pHluorin), SEP-GluA1 (27, 28), into single neurons to restrict the signal to membrane-inserted receptors, together with ChR2 and a volume-filling marker DsRed2. Because GFP-tagged proteins would occlude the GCaMP6s signal, we electroporated GCaMP6s alone into neighboring neurons to determine a pairing target location for inducing plasticity in the ChR2+ neuron (Fig. 4A). Indeed neighboring neurons in V1 share a substantial proportion of their subthreshold receptive field (Fig. S10). A strong and distinct SEP fluorescence signal was observed at the surface of individual spines (Fig. 4B, left). Comparing changes in SEP-GluA1 enrichment with volume changes in individual spines more than two hours after the pairing protocol, we found a significant positive correlation (Fig. 4C-E). Positive or negative changes in volume thus reflect corresponding modifications of spine synaptic weight through AMPAR expression changes.

The immediate early gene Arc is involved in AMPAR endocytosis (29). Arc preferentially interacts with the β isoform of CaMKII and acts as an inverse tag of plasticity (30) that could potentially mediate heterosynaptic depression in dendritic segments (31). We used a monomeric EGFP-tagged Arc (mEGFP-Arc) probe to study the molecular dynamics of Arc following the pairing protocol (30) (Fig. 4B, right). Arc enrichment in spines was increased in sLTD spines and decreased in sLTP spines (Fig. 4C-E). To test if Arc mediates heterosynaptic depression, we delivered small hairpin RNA (shRNA, Fig. S11 and S12) to deplete Arc in single neurons. Neurons in which Arc was knocked down displayed spines filled with SEP-GluA1 (Fig. 4F) which were homogenously distributed along dendrites compared to control neurons (Fig. 4G-H). To relate Arc expression to calcium signaling in spines (30) (Fig. S13), we additionally knocked down CaMKIIβ (Fig. S11). Dendrites with reduced CaMKIIβ displayed reduced spine-specific Arc expression (Fig. 4I-K). Knock-down of Arc in neurons expressing GCaMP6s and ChR2 prevented displacement of receptive fields toward the target after pairing (Fig. 4L and S12), consistent with impaired functional plasticity (32). In contrast to control neurons, the density of sLTP spines was not significantly different from the density of sLTD spines for neurons with Arc knock-down (Fig. 4M; see also Fig. S14). The spatial organization of sLTD spines around sLTP spines was impaired in Arc knock-down dendrites compared to control (Fig. 4N), demonstrating that Arc helps organize the distribution of potentiated and depressed spines that underlies plasticity of neuronal responses. Local bi-directional plasticity of functionally identified spines was also observed in experiments where vision from the deprived eye was restored after monocular deprivation (Fig. S15). Thus, Arc-mediated heterosynaptic plasticity takes place under physiological conditions, and constitutes a mechanism for local coordination of synaptic plasticity that drives functional plasticity of neurons with heterogeneous synaptic inputs (Fig. S16).

## Supplementary Material

Refer to Web version on PubMed Central for supplementary material.

## Acknowledgements:

We thank Rachael Neve, Benjamin Bartelle and Alan Jasanoff for their assistance with plasmid preparation and testing. We thank Jeremy Petravicz for performing the eyelid sutures for MD experiments, Murat Yildirim for providing two-photon point spread function measurements and Keji Li for his assistance with optical intrinsic imaging. We thank Olivier Marre, Johannes Mayrhofer and Celia Gasselin for their comments on the manuscript. We thank Vivek Jayaraman, Rex A. Kerr, Douglas S. Kim, Loren L. Looger and Karel Svoboda from the GENIE Project, Janelia Farm Research Campus, Howard Hughes Medical Institute (HHMI) for the distribution of GCaMP6.

Funding:

This work was supported by Marie Curie postdoctoral fellowship FP7-PEOPLE-2010-IOF (S.E.B.), Human Frontier Science Program Long-Term Fellowship (J.P.K.I), AMED-CREST (H.B.) and KAKENHI grants (15H04258 to H.O., 15H02358 and 17H06312 to H.B.), and NIH grants NS090473 and EY007023; NSF grant EF1451125; the Simons Center for the Social Brain; and the Picower Institute Innovation Fund (M.S.).

## References and Notes:

1. Ko H et al., The emergence of functional microcircuits in visual cortex. Nature. 496, 96–100 (2013). [PubMed: 23552948]
2. Espinosa JS, Stryker MP, Development and plasticity of the primary visual cortex. Neuron. 75, 230–49 (2012). [PubMed: 22841309]
3. Chen SX, Kim AN, Peters AJ, Komiyama T, Subtype-specific plasticity of inhibitory circuits in motor cortex during motor learning. Nat. Neurosci. 18, 1109–1115 (2015). [PubMed: 26098758]
4. Cichon J, Gan W-B, Branch-specific dendritic Ca2+ spikes cause persistent synaptic plasticity. Nature. 520, 180–185 (2015). [PubMed: 25822789]
5. Hayashi-Takagi A et al., Labelling and optical erasure of synaptic memory traces in the motor cortex. Nature. 525, 333–8 (2015). [PubMed: 26352471]
6. Turrigiano GG, Nelson SB, Homeostatic plasticity in the developing nervous system. Nat. Rev. Neurosci. 5, 97–107 (2004). [PubMed: 14735113]
7. Ibata K, Sun Q, Turrigiano GG, Rapid Synaptic Scaling Induced by Changes in Postsynaptic Firing. Neuron. 57, 819–826 (2008). [PubMed: 18367083]
8. Ju W et al., Activity-dependent regulation of dendritic synthesis and trafficking of AMPA receptors. Nat. Neurosci. 7, 244–253 (2004). [PubMed: 14770185]
9. Oh WC, Parajuli LK, Zito K, Heterosynaptic Structural Plasticity on Local Dendritic Segments of Hippocampal CA1 Neurons. Cell Rep. 10, 162–169 (2015). [PubMed: 25558061]
10. Sutton MA et al., Miniature Neurotransmission Stabilizes Synaptic Function via Tonic Suppression of Local Dendritic Protein Synthesis. Cell. 125, 785–799 (2006). [PubMed: 16713568]
11. Bian W-J, Miao W-Y, He S-J, Qiu Z, Yu X, Coordinated Spine Pruning and Maturation Mediated by Inter-Spine Competition for Cadherin/Catenin Complexes. Cell. 162, 808–822 (2015). [PubMed: 26255771]
12. Winnubst J, Cheyne JE, Niculescu D, Lohmann C, Spontaneous Activity Drives Local Synaptic Plasticity In Vivo. Neuron. 87, 399–410 (2015). [PubMed: 26182421]
13. Bourne JN, Harris KM, Coordination of Size and Number of Excitatory and Inhibitory Synapses Results in a Balanced Structural Plasticity Along Mature Hippocampal CA1 Dendrites During LTP. 373, 354–373 (2011).
14. Govindarajan A, Kelleher RJ, Tonegawa S, A clustered plasticity model of long-term memory engrams. Nat. Rev. Neurosci. 7, 575–583 (2006). [PubMed: 16791146]
15. Béïque J, Na Y, Kuhl D, Worley PF, Huganir RL, Arc-dependent synapse-specific homeostatic plasticity. Proc. Natl. Acad. Sci. U. S. A. 108, 816–21 (2011). [PubMed: 21187403]
16. Hou Q, Zhang D, Jarzylo L, Huganir RL, Man H-Y, Homeostatic regulation of AMPA receptor expression at single hippocampal synapses. Proc. Natl. Acad. Sci. U. S. A. 105, 775–780 (2008). [PubMed: 18174334]
17. Lee MC, Yasuda R, Ehlers MD, Metaplasticity at Single Glutamatergic Synapses. Neuron. 66, 859–870 (2010). [PubMed: 20620872]

18. Rabinowitch I, Segev I, Two opposing plasticity mechanisms pulling a single synapse. Trends Neurosci. 31, 377–383 (2008). [PubMed: 18602704]
19. Supplementary Online Materials.
20. Meliza CD, Dan Y, Receptive-field modification in rat visual cortex induced by paired visual stimulation and single-cell spiking. Neuron. 49, 183–189 (2006). [PubMed: 16423693]
21. Pawlak V, Greenberg DS, Sprekeler H, Gerstner W, Kerr JND, Changing the responses of cortical neurons from sub- To suprathreshold using single spikes in vivo. Elife. 2013, 1–18 (2013).
22. Chen T-W et al., Ultrasensitive fluorescent proteins for imaging neuronal activity. Nature. 499, 295–300 (2013). [PubMed: 23868258]
23. Zhang F et al., Multimodal fast optical interrogation of neural circuitry. Nature. 446, 633–639 (2007). [PubMed: 17410168]
24. Matsuzaki M, Honkura N, Ellis-Davies GCR, Kasai H, Structural basis of long-term potentiation in single dendritic spines. Nature. 429, 761–766 (2004). [PubMed: 15190253]
25. Harvey CD, Svoboda K, Locally dynamic synaptic learning rules in pyramidal neuron dendrites. Nature. 450, 1195–1200 (2007). [PubMed: 18097401]
26. Zhang Y, Cudmore RH, Lin D-T, Linden DJ, Huganir RL, Visualization of NMDA receptor–dependent AMPA receptor synaptic plasticity in vivo. Nat. Neurosci, 1–8 (2015). [PubMed: 25547471]
27. Kopec CD, Li B, Wei W, Boehm J, Malinow R, Glutamate receptor exocytosis and spine enlargement during chemically induced long-term potentiation. J. Neurosci. 26, 2000–2009 (2006). [PubMed: 16481433]
28. Makino H, Malinow R, Compartmentalized versus global synaptic plasticity on dendrites controlled by experience. Neuron. 72, 1001–1011 (2011). [PubMed: 22196335]
29. Chowdhury S et al., Arc/Arg3.1 Interacts with the Endocytic Machinery to Regulate AMPA Receptor Trafficking. Neuron. 52, 445–459 (2006). [PubMed: 17088211]
30. Okuno H et al., Inverse synaptic tagging of inactive synapses via dynamic interaction of Arc/Arg3.1 with CaMKIIβ. Cell. 149, 886–898 (2012). [PubMed: 22579289]
31. Mullins C, Fishell G, Tsien RW, Unifying Views of Autism Spectrum Disorders: A Consideration of Autoregulatory Feedback Loops. Neuron. 89, 1131–1156 (2016). [PubMed: 26985722]
32. McCurry CL et al., Loss of Arc renders the visual cortex impervious to the effects of sensory experience or deprivation. Nat. Neurosci. 13, 450–457 (2010). [PubMed: 20228806]
33. Knott GW, Holtmaat A, Wilbrecht L, Welker E, Svoboda K, Spine growth precedes synapse formation in the adult neocortex in vivo. Nat. Neurosci. 9, 1117–1124 (2006). [PubMed: 16892056]

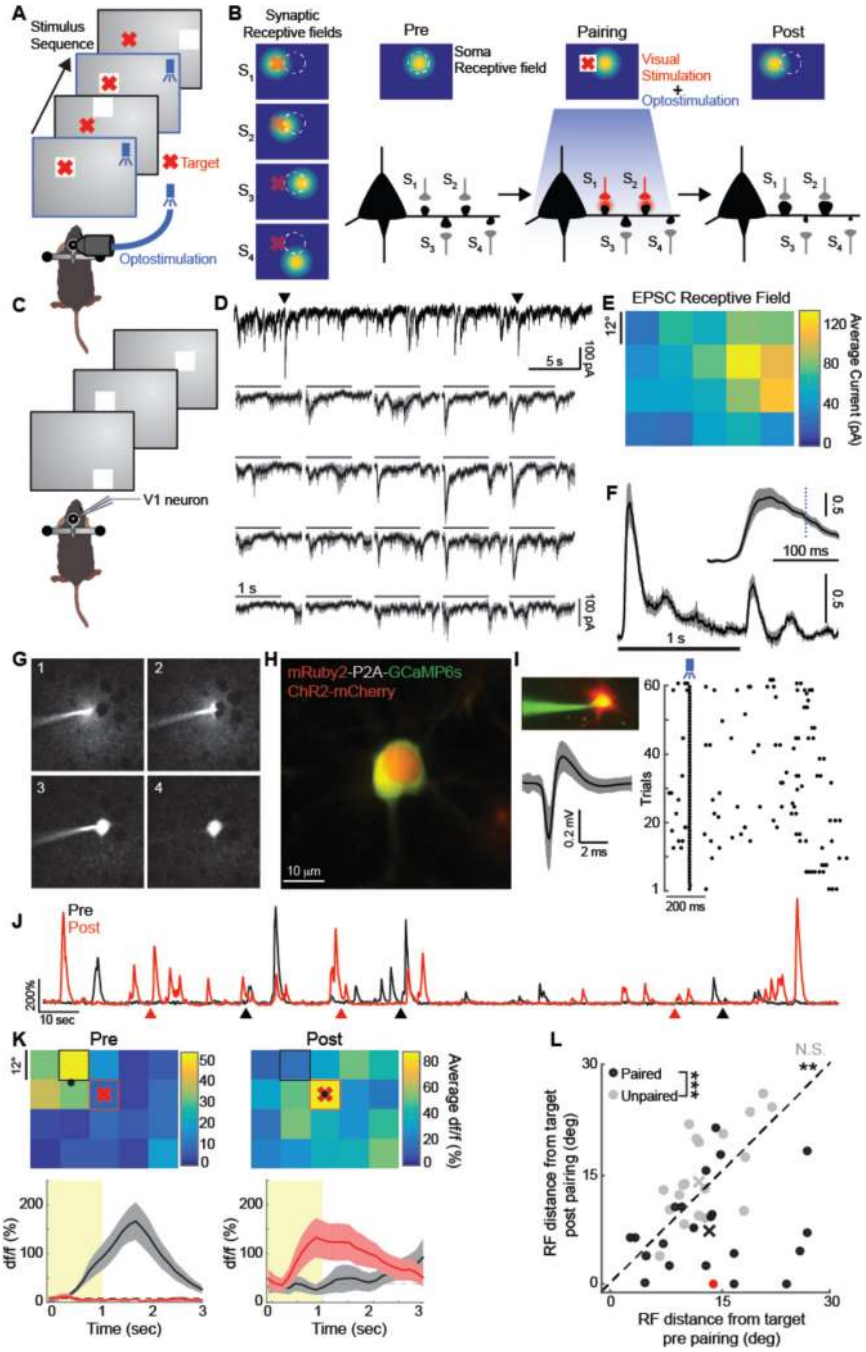


**Fig. 1. Induction of receptive field plasticity in V1 neurons.**

(**A**) Pairing protocol. (**B**) Effect of pairing on a neuron's receptive field and its dendritic spines ($S_1$-$S_4$). (**C**) Whole-cell recording during sparse noise stimuli. (**D**) Top: Excitatory current trace of a recorded neuron. Bottom: Average EPSC for each stimulus location. (**E**) Receptive field obtained by averaging EPSCs between 50–150ms. (**F**) EPSC in z-score averaged over all neurons and stimulus locations (n=8 neurons). Dashed blue line: 150ms. (**G**) Single-cell electroporation *in vivo*. (**H**) Neuron expressing mRuby2-P2A-GCaMP6s and ChR2-mCherry. (**I**) Loose-patch recording of a ChR2+ neuron spiking to single blue light

pulses. Spike waveforms are shown (grey: standard deviation). (**J**) Calcium df/f traces obtained from soma. Arrows: onset of visual stimuli, presented pre-pairing at the preferred location (black) and post-pairing at the target location (red). (**K**) Top: Receptive fields from **J** traces. Preferred stimulus locations shown with black (pre) and red (post) squares. Black dots: center-of-mass. Red crosses: target stimulus. Bottom: Response time course in squared locations. Shaded areas: s.e.m. (**L**) Distance between target and receptive field center-of-mass pre- and post-pairing (black, n=22 neurons, N=23 mice, paired Wilcoxon test, ** $p<0.01$). Red dot: example in panel **K**. Cross: average shift. Control neurons with unpaired ChR2 visual stimulation shown in gray (n=21 neurons, N=11 mice, p=0.06, N.S. Not significant). Receptive field shifts were significantly different between paired and unpaired populations (unpaired Kruskal-Wallis test, *** $p<0.001$).

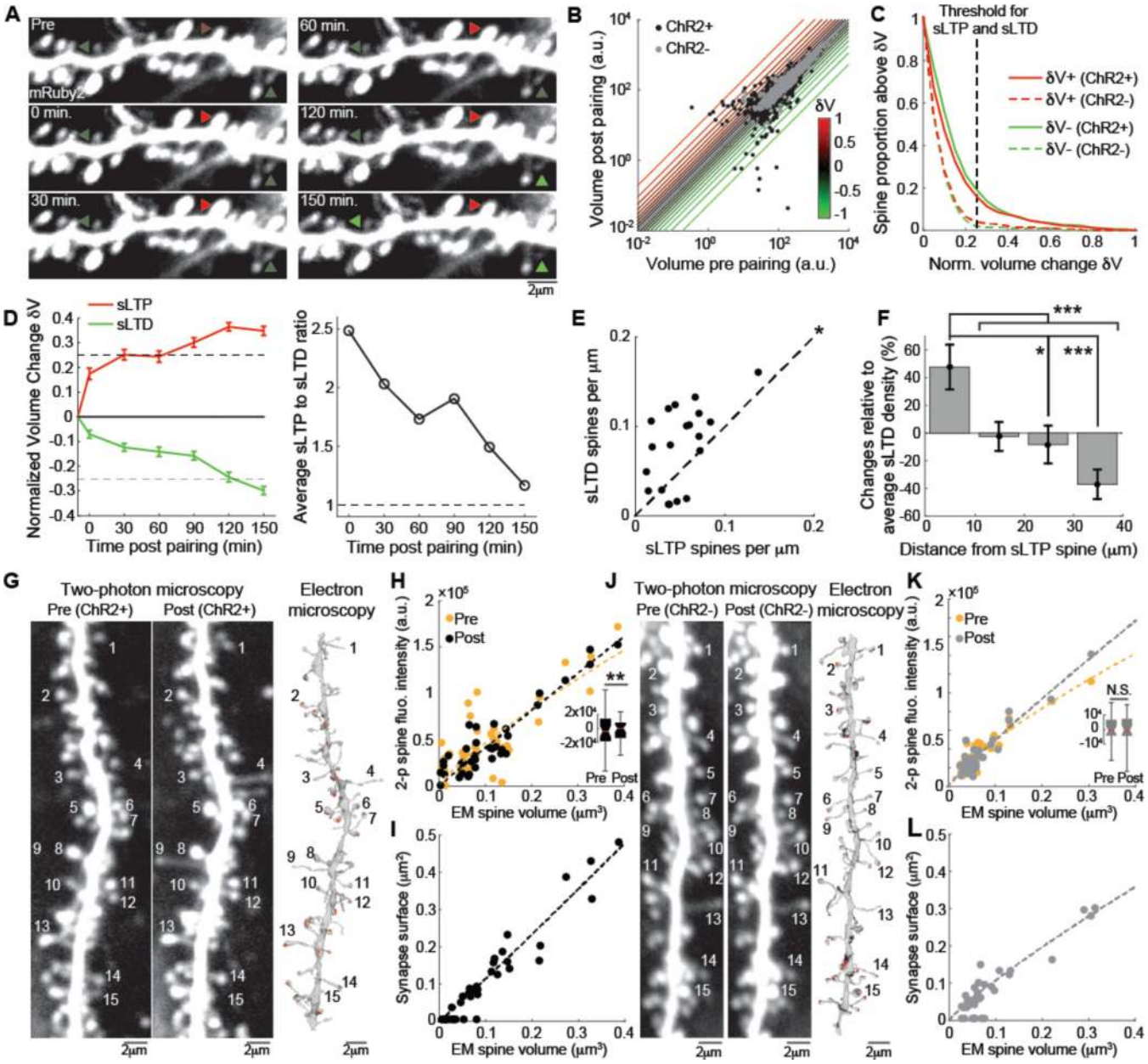


**Fig. 2. Hebbian potentiation and heterosynaptic depression in stretches of dendrite.**

(**A**) Time-lapse dendritic imaging. (**B**) Spine volumes pre- and post- (>2h) pairing for ChR2+ (n=1987 spines) and ChR2− (n=845 spines) neurons. (**C**) Proportion of enlarged (δV +) and shrunken (δV−) spines above different δV values (variance F-test between ChR2+ and ChR2−, $p<0.001$). Black dashed line: sLTP and sLTD threshold δV= ±0.25. (**D**) Left: average normalized volume change over time for sLTP (n=110) and sLTD (n=98) spines. Dashed lines: threshold. Right: sLTP-to-sLTD volume change ratio. (**E**) sLTP and sLTD spine density per dendrite (n=20 dendrites; Pearson coefficient: 0.55, $p<0.05$; paired Wilcoxon test, *$p<0.05$). (**F**) sLTD spine density variation relative to mean as a function of distance from sLTP spines (n=103 sLTP spines, one-way ANOVA test, $p<0.01$, unpaired Kruskal-Wallis test, ***$p<0.001$ and *$p<0.05$ with Bonferroni correction). (**G**) ChR+

dendrite imaged pre- and post-pairing and reconstructed by EM after the experiment, post-pairing. (**H**) Spine volume measured with EM compared to two-photon fluorescence signal (n = 36 spines, EM versus post: $r^2 = 0.85$, EM versus pre: $r^2 = 0.57$). Lines depict best-fit power functions. Inset: distribution of fit residuals (unpaired variance F-test, **p<0.01). (**I**) Spine volume versus synaptic surface area (n=36, $r^2 = 0.91$). Note that some small spines lacked synapses, as previously reported (33). (**J**-**L**) Same as **G-I** for a ChR- neuron (n = 33 spines, EM versus post: $r^2 = 0.88$, EM versus pre: $r^2 = 0.85$, unpaired variance F-test, N.S. Not significant). Spine volume versus synapse area (n=39, $r^2 = 0.92$). Error bars: s.e.m.

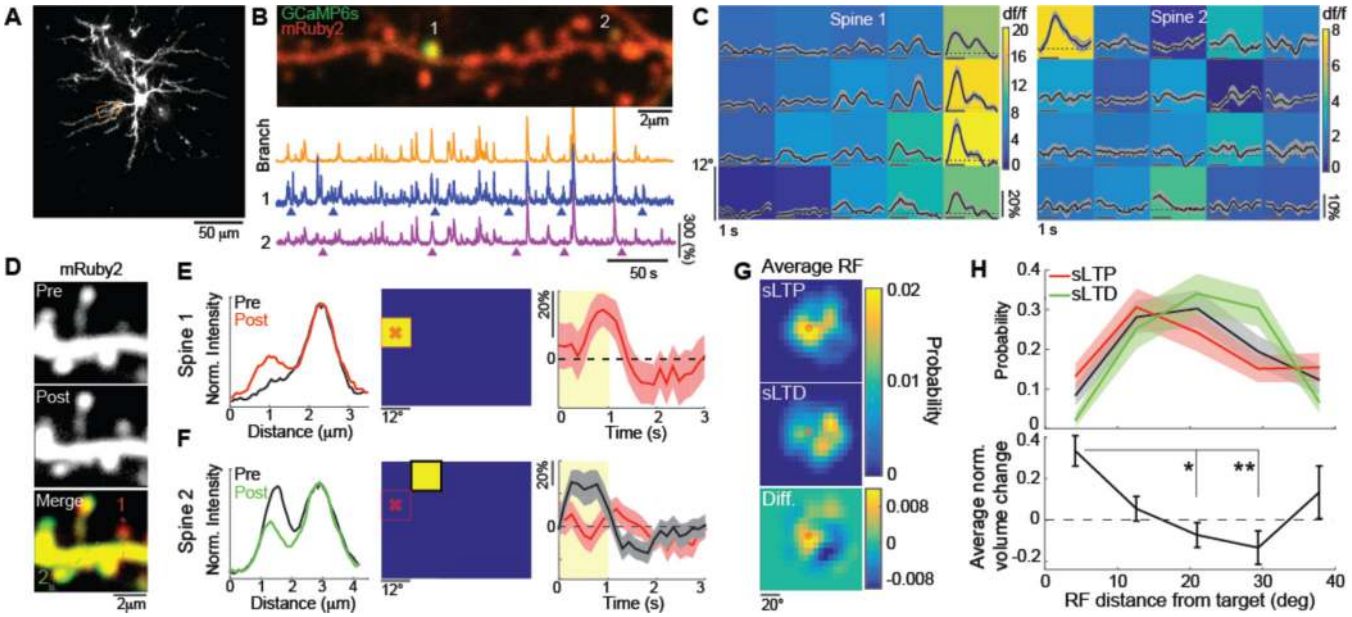


**Fig. 3. Functional identification of sLTP and sLTD dendritic spines.**

(**A**) Neuron expressing mRuby2-P2A-GCaMP6s. (**B**) Top: Dendritic stretch from **A**. Bottom: Calcium traces for two spines and branch. Arrows: onset of preferred stimuli. (**C**) Receptive fields for spines in **B**. Shaded gray: s.e.m. Colormap: time-averaged response. (**D**) Dendritic segment with nearby sLTP (1) and sLTD (2) spines. (**E**) Left: Profiles from dashed red line in **D**. Middle: receptive field of the spine. Red cross: target position. Right: Response time course for the preferred stimulus. Shaded areas: s.e.m (**F**) Same as **E** for sLTD spine in **D**. Right: Response time course for the preferred stimulus (gray) and for the target stimulus location (red). (**G**) Average normalized receptive field centered on target for sLTP (n=94) and sLTD (n=87) spines. Bottom: difference between distributions. (**H**) Top: Distribution of receptive field distances from target. Black distribution: randomized spine identity. Shaded areas: standard deviation. Bottom: Average normalized volume change as a function of receptive field distance from target for all sLTP and sLTD spines (n=181 spines, one-way ANOVA test, $p<0.01$, * $p<0.05$ and ** $p<0.01$ with Bonferroni correction). Error bars: s.e.m.

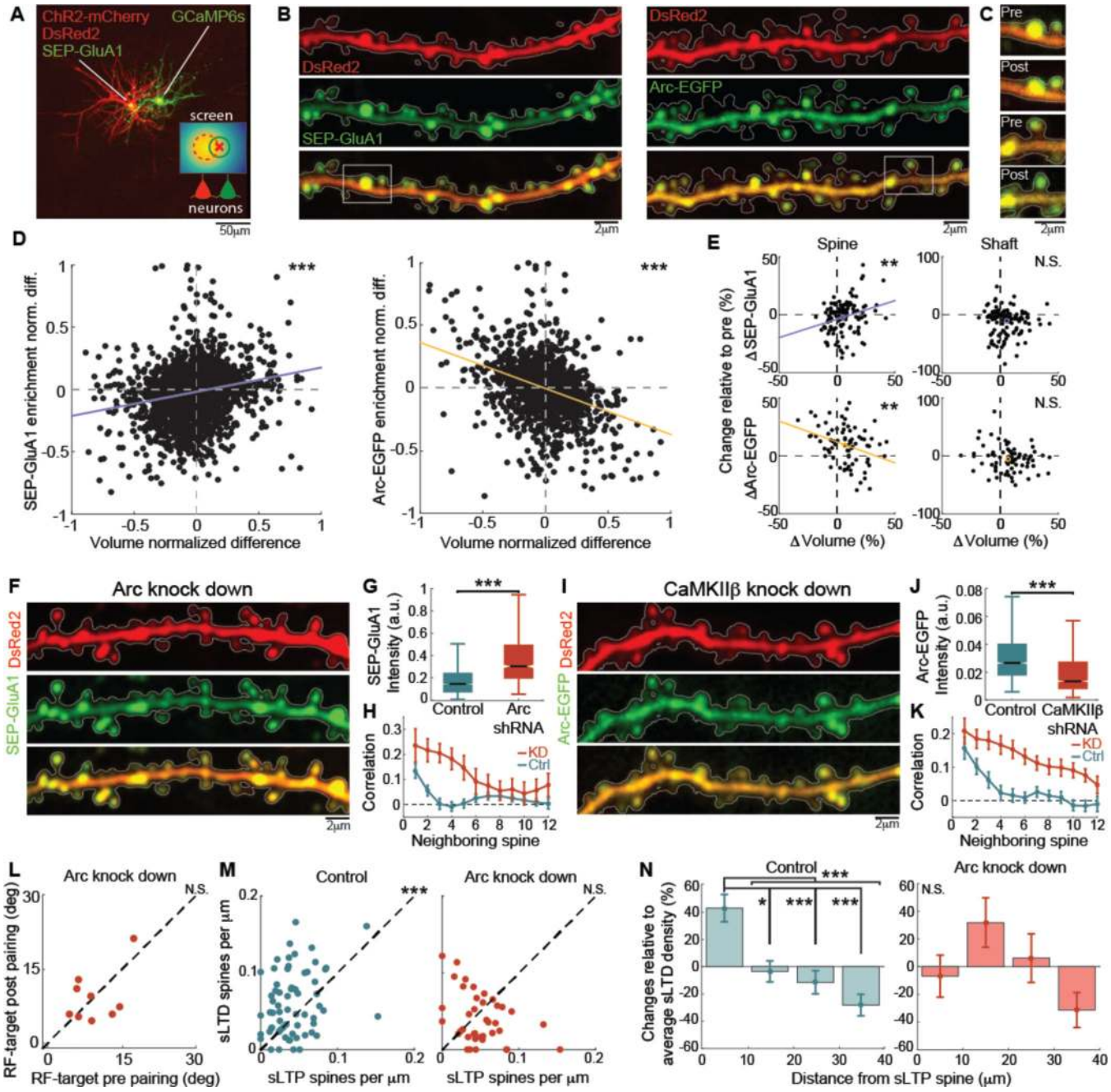


**Fig. 4. Role of Arc in regulating plasticity of V1 neurons.**

(**A**) Neuron expressing ChR2-mCherry, DsRed2 and SEP-GluA1 in close proximity to a neuron expressing GCaMP6s. (**B**) Dendrites expressing SEP-GluA1 (left) or Arc-EGFP (right). (**C**) Spines corresponding to white rectangles in **B**. (**D**) Comparison between normalized change in volume and SEP-GluA1 (left) or Arc-EGFP (right) enrichment (SEP-GluA1: n=4354 spines from 17 neurons, N=12 mice, Pearson coefficient=0.22, *** p<0.001; Arc-EGFP: n=1719 spines from 16 neurons, N=8 mice, Pearson coefficient=−0.37, *** p<0.001). (**E**) Relative volume changes compared to relative SEP-GluA1 (top, n=122 dendrites) or Arc-EGFP (bottom, n=81 dendrites) enrichment changes averaged over all

spines or measured in the dendritic shaft (Pearson coefficient: 0.27, ** p<0.01 for SEP-GluA1 and −0.29, ** p<0.01 for Arc-EGFP, N.S. Not Significant). Purple and orange lines: best linear fits. Circles: average values. (**F**) Dendrite expressing SEP-GluA1 and Arc shRNA-DsRed2. (**G**) Distributions of spine SEPGluA1 average intensity when Arc is endogenously expressed or knocked down (n=960 spines from 3 neurons for KD, n=2669 spines from 11 neurons for Ctrl, Kruskal-Wallis test, *** p <0.001). (**H**) SEP-GluA1 intensity correlation with neighboring spines. (**I-K**) Same as **F-H** in control or CaMKIIβ KD dendrites expressing Arc-EGFP (n=2053 spines from 4 neurons for KD, n=2550 spines from 11 neurons for Ctrl, Kruskal-Wallis test, *** p <0.001). (**L**) Distance between target and receptive field pre and post pairing for the KD condition (n=9 neurons, N=7 mice, paired Wilcoxon test, N.S. not significant). (**M**) sLTP and sLTD spine density per dendrite for control (n=66 dendrites; Pearson coefficient: 0.31, p<0.05; paired Wilcoxon test, *** p<0.001) and Arc KD neurons (n=39 dendrites; Pearson coefficient: −0.37, p<0.05; paired Wilcoxon test, N.S. Not Significant) conditions. (**N**) sLTD spine density variation relative to the mean as a function of distance from sLTP spines for the control (average over n=253 sLTP spines, one-way ANOVA test, p<0.001, unpaired Kruskal-Wallis test, ***p<0.001 and *p<0.05 with Bonferroni correction) and Arc KD conditions (average over n=142 sLTP spines, one-way ANOVA test, N.S. Not significant). Dendrites in the control condition either express a scrambled Arc shRNA plasmid fused with DsRed (n=46 dendrites) or mRuby2-P2A-GCaMP6s (n=20 dendrites).